Reactive nitrogen (NO_y) and ozone responses to energetic electron precipitation during Southern Hemisphere winter

Pavle Arsenovic[1,*], Alessandro Damiani[2], Eugene Rozanov[1,3,4], Bernd Funke[5], Andrea Stenke[1], Thomas Peter[1]

[1]Institute for Atmospheric and Climate Science ETH, Zürich, Switzerland
[2]Center for Environmental Remote Sensing (CEReS), Chiba University, Chiba, Japan
[3]Physikalisch-Meteorologisches Observatorium Davos – World Radiation Center, Davos, Switzerland
[4]Pushkov Institute of Terrestrial Magnetism, Ionosphere, and Radio Wave Propagation, Russian Academy of Sciences, Kaliningrad, Russia
[5]Instituto de Astrofisica de Andalucía, CSIC, Granada, Spain
[*]Now at Empa, Dübendorf, Switzerland

Correspondence to: Pavle Arsenovic (pavle.arsenovich@gmail.com)

Abstract. Energetic particle precipitation (EPP) affects the chemistry of the polar middle atmosphere by producing reactive nitrogen (NO_y) and hydrogen (HO_x) species, which then catalytically destroy ozone. Recently, there have been major advances in constraining these particle impacts through a parametrization of NO_y based on high quality observations. Here we investigate the effects of low (auroral) and middle (radiation belt) energy range electrons, separately and in combination, on reactive nitrogen and hydrogen species as well as on ozone during Southern Hemisphere winters from 2002 to 2010 using the chemistry-climate model SOCOL3-MPIOM. Our results show that, in absence of solar proton events, low energy electrons produce the majority of NO_y in the polar mesosphere and stratosphere. In the polar vortex, NO_y subsides and affects ozone at lower altitudes, down to 10 hPa. Comparing a year with high electron precipitation with a quiescent period, we found large ozone depletion in the mesosphere; as the anomaly propagates downward, 15 % less ozone is found in the stratosphere during winter, which is confirmed by satellite observations. Only with both low and middle energy electrons, our model reproduces the observed stratospheric ozone anomaly.

1 Introduction

Energetic particles originating from the Sun, the magnetosphere, or from outside the solar system continuously precipitate into the Earth's atmosphere and can influence atmospheric processes. They ionize neutral air molecules especially in the middle and upper polar atmosphere and create odd nitrogen and hydrogen species, NO_x ([N] + [NO] + [NO_2]) and HO_x ([H] + [OH] + [HO_2]). NO_x and HO_x radicals can catalytically deplete ozone. The *in-situ* destruction of ozone in the mesosphere is characteristic for HO_x due to its fast reaction rates (Bates and Nicolet, 1950). On the other hand, NO_x, in the absence of sunlight, subsides within the down-welling branch of the overturning circulation, affecting ozone concentrations at lower altitudes (Solomon *et al* 1982).

High energy particles, i.e. solar protons (Jackman *et al* 2008) and radiation belt electrons (Arsenovic *et al*, 2016; Semeniuk *et al* 2011) can penetrate directly into the mesosphere and stratosphere. Radiation belt electrons (energies > 30 keV) impact chemistry below 90 km in the atmosphere (Turunen *et al* 2009). Electrons of lower energies (< 30 keV, auroral) originate from the magnetosphere as well as the radiation belt electrons (Mironova *et al* 2015), but they get accelerated in the magnetotail and precipitate into the lower thermosphere in the auroral ovals (55 – 70° geomagnetic latitude) (Baker *et al* 2001; Barth *et al* 2003). Their peak impact is above 90 km in the thermosphere (Turunen *et al* 2009).

There have been numerous attempts to include low energy electrons (LEE) in climate models. Chemistry-climate or chemistry-transport models with top in the thermosphere, e.g. HAMMONIA (Schmidt *et al* 2006), KASIMA (Reddmann *et al* 2010) and WACCM (Andersson *et al* 2018; Marsh *et al* 2007), have included effects of LEE directly because they deposit their energy within the model domain. For climate models that have an upper lid below the thermosphere, a prescription of LEE either as NO_y influx through the model top or as concentrations (number density) in the upper model boxes is recommended (Matthes *et al* 2017). Baumgaertner *et al* (2009) has developed a parameterization of this flux based on the geomagnetic activity A_p index, a daily worldwide measure of the effects of solar wind on the Earth magnetic field. When incorporated into a chemistry-climate model, results showed significant ozone depletion in the mesosphere and stratosphere (Baumgaertner *et al* 2011). For the SOCOL chemistry-climate model Rozanov *et al* (2012) also found significant ozone decreases in the mesosphere and stratosphere, with peak values around 10 % in September around 36 km altitude over the Antarctic.

Funke *et al* (2016) have recently developed a semi-empirical model that calculates concentrations and fluxes of mesospheric and stratospheric NO_y compounds ($[NO] + [NO_2] + 2\times [N_2O_5] + [HNO_3] + [ClONO_2]$) based on the Michelson Interferometer for Passive Atmospheric Sounding (MIPAS) observations. The model exploits the nearly linear relationship in the mesosphere between A_p index with observed NO_y produced by EPP. This advance in the representation of LEE in climate models motivates us to investigate if LEE can have a larger impact on atmospheric chemistry than previously thought (Rozanov *et al* 2012). Moreover, this LEE parameterization is a part of the recommended solar forcing dataset for climate models within the upcoming Coupled Model Intercomparison Project Phase 6 (CMIP-6, Matthes *et al* 2017).

It is crucial to have a realistic representation of EPP in models as the introduced signal impacts atmospheric chemistry and potentially regional climate (Baumgaertner *et al* 2011; Maliniemi *et al* 2014; Rozanov *et al* 2012; Seppälä *et al* 2013). Sinnhuber *et al* (2018) showed the impact of one possible implementation of the new Funke *et al* (2016) LEE NO_y parameterization in their EMAC model on NO_y and ozone; however, they did not explicitly consider MEE. Here we present results from our state of the art chemistry-climate model employing a different implementation of the same parameterization of LEE together with the previous representations of other energetic particles. This paper focuses on evaluating NO_x and ozone response to LEE and MEE precipitation, separately and in combination, in Antarctic winters (JJA: June, July and August), in order to avoid the more complicated Arctic polar vortex with its high variability and strong dependence on meteorological conditions (Hitchcock *et al* 2013). We compare our results with the satellite observations.

2 Methods

We used the coupled chemistry-climate model SOCOL3-MPIOM (Muthers *et al* 2014; Stenke *et al* 2013). The atmospheric dynamic component of the model is ECHAM5.4 (Roeckner and Bäuml, 2003), coupled to the air chemistry module MEZON (Egorova *et al* 2003; Rozanov *et al* 1999) and the interactive ocean module MPIOM (Jungclaus *et al* 2006; Marsland *et al* 2002). We carried out the experiments with T31 spectral resolution on 39 vertical levels from the surface up to 0.01 hPa (~80 km).

The model boundary conditions and parameterizations are identical to those described in Arsenovic *et al* (2016), except for the LEE parameterization. Following Calisto *et al* (2011), galactic cosmic rays (GCR) are parameterized as a function of geomagnetic latitude, pressure and solar modulation potential. Ionization by solar protons (SP) is treated according to Jackman *et al* (2008) and ionization by middle energy electrons (MEE) with energies between 30 and 300 keV is taken from the Atmospheric Ionization Module Osnabrück (AIMOS) v1.6 (Arsenovic *et al* 2016; Wissing and Kallenrode, 2009). Electrons of energies higher than 300 keV are not included in the model due to a lack of adequate parameterization.

For LEE, we are using the semi-empirical model for NO_y influx by Funke *et al* (2016) through the model top at 0.01 hPa (75-80 km in polar conditions). Although MIPAS scans the atmosphere up to 68 km altitude, the applicability of this parameterization above 70 km has been validated by comparing to MIPAS Middle and Upper atmosphere observations (scanning up to 100 and 170 km, respectively). As more than 99 % of the NO_y at this altitude is in the form of nitrogen monoxide (nitric oxide), NO (Brasseur and Solomon, 2005), we approximate the NO_y influx calculated by the semi-empirical model as NO influx at this level in SOCOL3-MPIOM. As mentioned before, LEE precipitate above 90 km and MEE precipitate between 70 and 90 km altitude (Turunen *et al* 2009). However, because of our model top at 80 km, here we consider electrons that precipitate below 80 km as MEE and electrons that precipitate above model top as LEE.

Matthes *et al* (2017) and Sinnhuber *et al* (2018) also implemented the parameterization by Funke *et al* (2016) in the EMAC model. They used a different approach, prescribing NO concentrations (instead of fluxes through the model top) in the model within the 0.09 - 0.01 hPa layer and performed the simulations with specified dynamics. Prescribing concentrations requires overwriting NO simulated values. It is inconsistent with the treatment of the physical and chemical processes in our model leading to accumulation of NO_y. This is not the case for influx approach and therefore we prescribe the NO influx instead of NO concentrations, however prescribed NO concentrations can be used for models with different treatment of the chemical and transport processes.

Figure 1 shows the monthly mean geomagnetic A_p index that covers our simulated period. Period 2002-2005 was characterized by a rather high A_p index and the 2006-2010 period by low values. For our simulations, we have used daily NO fluxes calculated from daily A_p indices.

Four sets of 6-member ensemble simulations were carried out, covering the 2002-2010 period: the "ALL" simulation, that includes all energetic particles (GCR, SP, MEE and LEE), the "LEE" simulation (GCR, SP and LEE), the "MEE" simulation

(GCR, SP and MEE) and the reference, "REF" simulation (GCR and SP). All these simulations have the same model boundary conditions and differ only in the inclusion of the low/middle energy electron precipitation.

We used two satellite datasets to evaluate our model results: MIPAS for nitrogen species and the Microwave Limb Sounder (MLS) for ozone. MIPAS was a Fourier transform spectrometer aboard the ENVISAT satellite (Fischer *et al* 2008). The quality of MIPAS NO_y and individual NO_y species has been extensively assessed in SPARC (2017), as well as specific validation studies (e.g. Bender *et al* 2015; Sheese *et al* 2016). The top altitude of the MIPAS nominal limb scans is 68 km, but it also contains information on the NO_y above, though with low vertical resolution. Since it provides the entire NO_y budget in the upper atmosphere (with vertical resolution of 3-5 km), we used this dataset to validate simulated NO_y.

The MLS aboard the Aura satellite (Waters *et al* 2006) provided daily measurements of ozone profiles (Froidevaux *et al* 2008) in the middle and upper atmosphere since August 2004. We used MLS observations to evaluate modeled ozone. The vertical resolution of MLS O_3 (v4.2) is about 3 km in the stratosphere, increasing up to about 5 km in the mesosphere (Livesey *et al* 2018).

3 Results

3.1 NO_y enhancement propagation

Figure 2 shows the difference in NO_y concentration between the geomagnetically active year 2005 and the mean over the geomagnetically quiescent period 2006 – 2010 averaged over 70 – 90°S. Even though year 2003 on average has higher Ap, here we choose year 2005 as the geomagnetically active year. This allows us to compare modeled NOy and ozone using two different satellite datasets MIPAS and MLS (which is available only since 2005). MIPAS data are unavailable from September 2005 to the end of the year, but our main period of interest is JJA, which is well covered by the observations.

The MIPAS observations (Figure 2a) show a NO_y enhancement throughout the mesosphere and upper stratosphere. In terms of mixing ratio, the highest increase of 500 – 600 ppbv is found in the upper mesosphere around 0.01 hPa (~80 km). There, the highest monthly values are observed in June. In the following months, this anomaly descends and reaches lower levels. In July, the NO_y enhancement of around 10 ppbv reaches the upper stratosphere around 2 hPa, and the increase, although smaller, is visible all the way down to 10 hPa. In the following months, the MIPAS nominal data were unavailable due to special observation mode campaigns.

The ALL experiment (Figure 2b) shows a very similar pattern of NO_y as the observations. The NO_y increase of 500 – 600 ppbv in the upper mesosphere around 0.01 hPa is similar as in the MIPAS observations. However, the wintertime NO_y peak below is slightly overestimated in the model compared to MIPAS. This is particularly visible in the lower mesosphere in June, as the modeled 100 ppbv NO_y enhancement reaches 0.1 hPa. The mesospheric anomaly extends into the stratosphere, but remains confined to the upper stratosphere, above 10 hPa, as in observations. The modeled NO_y overestimation suggests that downward transport is somewhat too fast in the model, or the photochemical lifetime of NO_y is too long, or horizontal mixing with mid-latitudes is underestimated. The modeled NO_y enhancement in September stems from a SP event (NOAA, 2018). In

contradiction to our results, the EMAC model slightly underestimates NO_y even during polar summer, for two pressure levels, 0.1 and 1 hPa (Matthes *et al* 2017). Sinnhuber *et al* (2018) showed underestimation of NO_y in the upper mesosphere in EMAC and KASIMA models and overestimation of NO_y in 3dCTM model in southern hemisphere compared to MIPAS observations. The LEE simulation (Figure 2c) shows very similar anomalies as ALL. The largest differences are in the upper mesosphere,

5 where LEE anomalies reach around 400 ppbv, which is underestimated compared to 500-600 ppbv found in MIPAS and ALL. A second interesting difference compared to ALL is the SP event in September. In LEE simulation, it reaches around 60 ppbv, while in ALL it exceeds 100 ppbv. This difference is coming from increased MEE precipitation that coincided with the SP event (see Arsenovic *et al* 2016, Figure 1a). During strong SP events protons can contaminate the highest electron channel, so this channel is excluded from the AIMOS dataset (Yando *et al* 2011). Although some degree of contamination is still possible

10 in the lower channels, protons are not the sole cause of the increased NO_y in this SP event. Namely, SP events are often associated to large coronal mass ejections that form a shock in front of them. Once the shock hits the Earth if often leads to a geomagnetic storm which leads to acceleration of electrons of > 30 keV energies. Therefore, increased MEE precipitation often happens very shortly after SP event because the shock and the geomagnetic storm are related to the same coronal mass ejection driver (Asikainen and Ruopsa, 2016).

15 The MEE simulation (Figure 2d) is drastically different from MIPAS as well as the ALL and LEE simulations. Although NO_y enhancement in the modeled geomagnetically active year exists, it is significantly decreased compared with the previous results. The modeled NOy mesospheric anomaly peak is absent and enhancement of 10 ppbv does not reach the stratosphere. Nevertheless, although less intense, increased NO_y is present throughout the mesosphere and stratosphere, and the NO_y increase in September due to the SP event exceeds again 100 ppbv, as in the ALL simulation.

20 The reference run in Figure 2e shows NO_y increase due to the SP events in the year 2005. In this year, there were 6 observed SP events in the shown timeframe – May 14, June 16, July 14 and 27, August 22 and September 8 (NOAA, 2018). In the geomagnetically inactive period, 2006-2010, there were no observed SP events in the presented months. Therefore, by excluding electron precipitation, the SP events alone cannot reproduce the observed features.

From the presented, we conclude that the inclusion of only LEE was sufficient to reproduce most of the NO_y enhancements.

25 The MEE contribution to NO_y increases is minor and brings the model closer to observations mainly in the upper mesosphere. As coronal mass ejections drive SP events and they can have an impact on the precipitation from the outer Van Allen belt (Asikainen and Ruopsa, 2016; Pierrard and Lopez Rosson, 2016), MEE precipitation could significantly contribute to NO_y increases in such events.

3.2 O₃ anomaly propagation

30 In the study of Matthes *et al* (2017), ozone responses were evaluated by comparing high and low geomagnetic activity years and their estimate shows good agreement with satellite observations (Fytterer *et al* 2015). To evaluate our simulated ozone responses, we follow a similar approach as used in Matthes *et al* (2017), that is, we compared our simulations with observations from MLS. We analyzed the 2005 – 2010 period when both, simulation and MLS data, are available.

Ozone anomalies from MLS observations during the high geomagnetically active year are depicted in Figure 3a. They are calculated as the difference averaged over 70 – 90º S between the active year (2005) and the average of geomagnetically quiescent years (2006 – 2010) divided by the ozone averaged over the whole period (2005 – 2010). Observations show around 20 % less ozone in the upper mesosphere (< 0.1 hPa) occurring mostly in the JJA period. The exception is the SP event on September 8, 2005. It created an ozone anomaly of up to 80 % stretching throughout whole mesosphere. The mesosphere below 0.1 hPa does not show a statistically significant difference between the geomagnetically active and quiescent years in absence of SP events. The observed negative ozone anomaly appears again around the stratopause in late June and propagates downwards to nearly 10 hPa in early September. The peak ozone anomaly occurs in August around 3 hPa, reaching ~15 %. Our results agree with the results from previous modeling studies (Reddmann *et al* 2010; Rozanov *et al* 2012; Sinnhuber *et al* 2018) and observations (Damiani *et al* 2016; Fytterer *et al* 2015).

The ALL simulation (Figure 3b) shows a negative ozone anomaly in the mesosphere as well. However, the magnitude is generally higher (around 30 %) and it is present from May to September. The September 2005 SP event is visible in the model simulations as well and descends from around 1 hPa in late September, reaching 10 hPa in late October. A similar pattern, but less obvious, is seen in the observations. Ozone anomalies in the lower mesosphere (0.5 – 0.1 hPa) are more pronounced in the model than in MLS observations. This is particularly evident in June when the modeled upper-mesosphere anomaly appears to relate to the upper-stratospheric anomaly, in contrast to the observations. This suggest that HO_x production by MEE might be overestimated. In the upper stratosphere model simulations agree well with observations. The decrease propagates downwards, reaching approximately 10 hPa in August, with a peak around 15 % in good agreement with the observations.

Ozone anomalies in the LEE simulation are shown in Figure 3c. Negative ozone anomalies are present mostly in the upper mesosphere (above 0.3 hPa) and have similar magnitude to ALL. Although in the LEE simulation the mesospheric ozone anomaly is overestimated compared to MLS observations, the stratospheric anomaly is almost completely absent. This is surprising, as there are very similar NO_y anomalies in the ALL and LEE simulations (see Figure 2).

Our MEE simulation shows similar ozone anomalies compared to LEE (Figure 3d). The anomalies are confined to a region above 1 hPa and are somewhat reduced compared to LEE and ALL. Similar to LEE, the stratospheric ozone anomaly seen in the observations and ALL simulation is almost absent.

In REF simulation (Figure 3e) most of the ozone anomaly features seen in observations and ALL are missing. The only depletion of ozone in this simulation is caused by SP events in the year 2005. Most of the observed events (May 14, June 16, July 14 and 27, August 22 and September 8) are clearly visible.

A recent study based on CCM WACCM (Andersson *et al* 2018) showed ozone anomaly propagation differences between high-A_p and low-A_p winters in the Southern Hemisphere. Their results are comparable with our ALL and LEE simulations. Compared with our ALL simulation, their ozone anomaly in case of all EEP of around 7 % is lower and occurs later (in October as opposed to August). However, their LEE simulation does not show significant ozone anomaly in the stratosphere, which is also the case in our results. In the study of Sinnhuber *et al* (2018) the three analyzed models (3dCTM, KASIMA and EMAC) generally show good agreement with the satellite observations,.

3.3 EEP effect on NO_y, HO_x and O_3

To estimate the total effect of energetic electron precipitation on NO_y, HO_x and ozone, we calculated the differences of experiment simulations (ALL, LEE and MEE) and REF simulation for the geomagnetically active period (2002 – 2005) using the simulated monthly mean values. Note that this is an idealized comparison and it is not directly comparable with observations, as there is always some amount of particle precipitation in the atmosphere (Funke *et al* 2014), unlike in the LEE, MEE and REF simulations.

The zonal mean of austral winter (JJA) average NO_y differences between ALL and REF is shown in Figure 4a. In polar night, NO_y is transported to lower altitudes by descending air motion. Significant modeled NO_y enhancements are present in the whole mesosphere and upper stratosphere above 10 hPa. Around 0.01 hPa, EPP produced NO_y increases from 50 ppbv at around 60° S, where NO_y lifetime is decreased due to the sunlight, to more than 500 ppbv at the pole, in the polar night. The differences in HO_x between those two experiments are shown on Figure 4b. Increases are mostly confined to the upper mesosphere and they reach the maximum of around 5 ppbv. However, smaller (< 1ppbv) but statistically significant HO_x increase appears in lower mesosphere and upper stratosphere around 60° S. Increases of NO_y and HO_x impact the ozone chemistry. Figure 4c shows changes in ozone concentrations due to electron precipitation. Ozone is significantly reduced throughout the whole polar region above 10 hPa. There are two peaks of ozone anomaly. The maximum decrease of up to 65 % (350 – 400 ppbv) is located in the upper mesosphere. This decrease is more severe than in previous modeling studies (Rozanov *et al* 2012), but this is because we focus on the geomagnetically active winters, when EPP effects are much more pronounced. The magnitude of ozone depletion is gradually decreasing with height reaching ~15 % (>200 ppbv) at the stratopause. The second ozone depletion peak is located between 10 and 1 hPa, reaching 15 % (>400 ppbv). A similar ozone response as in ALL has been shown by Semeniuk *et al* (2011).

Figure 4d shows the difference between modeled NO_y in LEE and REF simulation. Similarly, as in Figure 2, modeled NO_y in LEE simulation is very similar as in ALL, confirming the fact that the most of the NO_y is coming from LEE. Slight reduction to ALL still exists, visible mostly at 0.1 hPa at 90° S. Here, the value of NO_y is 100 ppbv while it is somewhat more in Figure 4a. A second difference is the absence of the enhancement equatorward of 30° S which is present in Figure 4a. Increase of HO_x in case of LEE is illustrated on Figure 4e. Changes of HO_x are very small and statistically insignificant, except for a small (<1 ppbv) increase in the polar upper mesosphere. This is expected as LEE do not produce HO_x. The small increase could be explained by an increase of NO_y which causes small increases of background HO_x through the Verronen and Lehmann (2015) mechanism, where enhanced NO coming from EEP leads to HO_x repartitioning increasing HO_x concentrations. Figure 4f shows ozone changes due to the LEE. Similar ozone decrease pattern as in Figure 4c exists but with a reduced intensity. The upper-mesospheric reduction reaches 35 % (~200 ppbv) and the upper-stratospheric anomaly is halved compared to ALL (200 ppbv $\triangleq$ 10 %). The absence of HO_x increases and reduced ozone anomalies compared to ALL illustrates the importance of MEE.

Figure 4g shows an increase of NO_y due to the MEE. Although MEE cause increases of NO_y, modeled NO_y is significantly reduced in the whole area compared to LEE and ALL simulation. In the upper mesosphere, this increase is around 50 ppbv, or a tenth of the total produced NO_y in ALL simulation. Between 30°-35° S NO_y enhancement is present again, as in ALL simulation. This enhancement is coming from the fact that MEE do not necessarily precipitate inside the polar vortex, as they precipitate in the sub-auroral ovals, which are centered around the geomagnetic pole. In contrast, NO_y coming from LEE descends into the mesosphere in the down-welling air motion inside of the polar vortex. The sum of NO_y increases (not shown) due to the LEE (Fig 4d) and due to the MEE (Fig 4g) closely reassembles NO_y increase as in the ALL case (Fig 4a).

Increases of HO_x due to MEE are presented in Figure 4h. Enhancements are present mostly in the upper mesosphere reaching 4 ppbv. The position and intensity of HO_x is very similar to ALL, but somewhat reduced. Because MEE produce OH, neglecting MEE in climate models would lead to an underestimation of HO_x; neglecting LEE would also lead to an underestimation of HO_x through the changed HO_x partitioning (Verronen and Lehmann, 2015). Changes in ozone concentrations due to MEE are shown in Figure 4i. Negative ozone anomalies are present in the mesosphere and in the upper stratosphere, albeit the stratospheric anomaly is statistically not significant. The biggest reduction with 35 % (~200 ppbv) is visible in the upper mesosphere. The anomaly in the upper stratosphere (10 – 1 hPa) does not exceed 100 ppbv. Interestingly, summing stratospheric ozone anomaly from LEE (Fig 3f) and from MEE (Fig 3i) does not reproduce ALL ozone anomaly (Fig 3c). The sum of the LEE and MEE ozone anomaly accounts for around 300 ppbv, while ALL shows about 400 ppbv between 10 and 1 hPa. Since the sum of enhanced NO_y due to LEE and MEE corresponds to ALL NO_y and HO_x enhancements occur in mesosphere, this discrepancy in ozone anomaly cannot be chemically explained. It could be caused by changes in dynamics (polar vortex strength) and temperature (which affects reaction rates).

Our results indicate that LEE and MEE are equally responsible for the ozone anomaly in the mesosphere. LEE deplete ozone through the production of large amounts of NO_y, while MEE contribute to the anomaly mostly through production of HO_x, which is the more efficient ozone destructor (Brasseur and Solomon 2005). Both LEE and MEE produce the stratospheric anomaly; however, LEE, through the production of large amounts of NO_y are more important.

4 Conclusions

We used the period 2005-2010 comprising intervals of high and low geomagnetic activity, which is well characterized by stratospheric and mesospheric measurements of NO_y and O_3, to investigate the accuracy of representations of energetic particle forcing in a chemistry-climate model. We assessed the impact of employing a new parameterization of LEE (< 30 keV) recommended for CMIP-6 in combination with the AIMOS parameterization for MEE (30 – 300 keV) on the simulated NO_y, HO_x and ozone variability. We used the SOCOL3-MPIOM climate model and focused on the Southern Hemispheric winter season. We compared NO_y with stratospheric and mesospheric MIPAS observations. The model captures the main features very well, but shows some differences in the winter maxima. LEE can reproduce most of the NO_y features, without including

MEE. However, increased MEE precipitation coincident with SP events may be a significant contribution to the observed NO_y amounts.

Simulated ozone depletion has been compared to MLS satellite observations, showing that patterns of ozone anomalies during the high EPP year 2005 compared to 2006-2010 match reasonably well. The model overestimates mesospheric ozone anomalies, but in the stratosphere a good match is accomplished. Ozone depletion of up to 15 % is found during July and August and reaches into the lower stratosphere. In essence, without including both LEE and MEE, the stratospheric anomaly cannot be accurately modeled. Future work is required to address the roles of indirect changes in temperature and dynamics in the EPP-induced stratospheric ozone variation.

Most of the NO_y in the mesosphere and stratosphere is produced by LEE in the upper mesosphere and lower thermosphere (<0.01 hPa) and transported downwards. A smaller fraction, namely ~10 %, is generated in-situ by ionization due to precipitating electrons of higher energies. These electrons play an important role because they produce HO_x, which depletes ozone near the HO_x source region in the mesosphere. Although not producing HO_x directly, LEE increase NO_y concentrations, which then causes repartitioning of HO_x and an increase in the HO_x lifetime (Verronen and Lehmann, 2015).

In summary, LEE and MEE lead to a reduction of ozone throughout the mesospheric and stratospheric polar region with a maximum percentage ozone depletion in the mesosphere (-65 %) and a second peak anomaly in the upper stratosphere (-15 %) with respect to the simulation where they are omitted. These chemical EPP signals can cause dynamical changes in the stratosphere that propagate into the lower atmosphere, which eventually affect regional climate (Rozanov *et al* 2012). Therefore, we recommend including both LEE and MEE in climate models.

Data availability

Due to the size limitations, SOCOL3-MPIOM model code, model boundary conditions and satellite data are only available upon request. The model output analyzed in this study can be found at https://data.mendeley.com/datasets/kgzwjgf4bk/1 (Arsenovic, 2019).

5   **Competing interests**

The authors declare that they have no conflict of interest.

Author contribution

PA and ER proposed the idea and designed the experiments; PA carried out the simulations and prepared the manuscript. AD analyzed MLS data and made Figure 3. BF provided MIPAS data. TP formulated the general line of research and supervised
10   the project. All authors provided critical feedback and helped shape the research, analysis and manuscript.

Acknowledgments

This work has been supported by the Swiss National Science Foundation under Grant CRSII2-147659 (FUPSOL II). AD was supported by JST/CREST/EMS/TEEDDA fund (JPMJCR15K4) and FONDECYT (Preis 1171690). BF was supported by the Spanish MCINN (ESP2017-87143-R) and EC FEDER funds. ER was supported by the Russian Science Foundation (17-17-
15   01060). This work is a part of ROSMIC WG1 activity within the SCOSTEP VarSITI program and WG3 and 5 activities within SPARC SOLARIS-HEPPA project. The authors thank NASA Goddard Earth Science Data and Information Services Center (GES DISC) for providing Aura/MLS data (https://mls.jpl.nasa.gov/), Timo Asikainen (University of Oulu) for clarification of the MEE/SP events relationship, Marina Dütsch (University of Washington) and Jelisaveta Arsenovic for assistance with improving the graphics, Amewu Mensah (ETH, Zürich) and William Ball (PMOD/WRC, Davos and ETH, Zürich) for
20   correcting the language. We thank our editor, Gabriele Stiller, Svenja Lange and three anonymous reviewers whose comments significantly improved the quality of this paper.

References

Andersson, M. E., Verronen, P. T., Marsh, D. R., Seppälä, A., Päivärinta, S. M., Rodger, C. J., Clilverd, M. A., Kalakoski, N. and van de Kamp, M.: Polar Ozone Response to Energetic Particle Precipitation Over Decadal Time Scales: The Role of
25   Medium-Energy Electrons, J. Geophys. Res. Atmos., 123(1), 607–622, doi:10.1002/2017JD027605, 2018.

Arsenovic, P.: SOCOL3-MPIOM model output, Mendeley Data, v1, http://dx.doi.org/10.17632/kgzwjgf4bk.1, 2019.

Arsenovic, P., Rozanov, E., Stenke, A., Funke, B., Wissing, J. M., Mursula, K., Tummon, F. and Peter, T.: The influence of Middle Range Energy Electrons on atmospheric chemistry and regional climate, J. Atmos. Solar-Terrestrial Phys., 149, 180–190, doi:10.1016/j.jastp.2016.04.008, 2016.

Asikainen, T. and Ruopsa, M.: Solar wind drivers of energetic electron precipitation, J. Geophys. Res. Sp. Phys., 121(3), 2209–2225, doi:10.1029/2002JA009458, 2016.

Baker, D. N., Barth, C. A., Mankoff, K. E., Kanekal, S. G., Bailey, S. M., Mason, G. M. and Mazur, J. E.: Relationships between precipitating auroral zone electrons and lower thermospheric nitric oxide densities: 1998–2000, J. Geophys. Res., 106(A11), 24,465-24,480, doi:2001JA000078, 2001.

Barth, C. A., Mankoff, K. D., Bailey, S. M. and Solomon, S. C.: Global observations of nitric oxide in the thermosphere, J. Geophys. Res. Sp. Phys., 108(A1), 1–11, doi:10.1029/2002JA009458, 2003.

Bates, D. and Nicolet, M.: The photochemistry of atmospheric water vapor, J. Geophys. Res., (55(3)), 301–327, doi:10.1029/JZ055:003p00301, 1950.

Baumgaertner, A. J. G., Jöckel, P. and Brühl, C.: Energetic particle precipitation in ECHAM5/MESSy1-Part 1: Downward transport of upper atmospheric NOxproduced by low energy electrons, Atmos. Chem. Phys., 9(8), 2729–2740, doi:10.5194/acp-9-2729-2009, 2009.

Baumgaertner, A. J. G., Seppälä, A., Jöckel, P. and Clilverd, M. A.: Erratum: Geomagnetic activity related NOx enhancements and polar surface air temperature variability in a chemistry climate model: Modulation of the NAM index (Atmospheric Chemistry and Physics (2011) 11 (4521-4531)), Atmos. Chem. Phys., 11(10), 4687, doi:10.5194/acp-11-4687-2011, 2011.

Bender, S., Sinnhuber, M., Von Clarmann, T., Stiller, G., Funke, B., López-Puertas, M., Urban, J., Pérot, K., Walker, K. A. and Burrows, J. P.: Comparison of nitric oxide measurements in the mesosphere and lower thermosphere from ACE-FTS, MIPAS, SCIAMACHY, and SMR, Atmos. Meas. Tech., 8(10), 4171–4195, doi:10.5194/amt-8-4171-2015, 2015.

Brasseur, G. P. and Solomon, S.: Aeronomy of the middle atmosphere: Chemistry and physics of the stratosphere and mesosphere, Springer, Dordrect, The Netherlands., 2005.

Calisto, M., Usoskin, I., Rozanov, E. and Peter, T.: Influence of Galactic Cosmic Rays on atmospheric composition and dynamics, Atmos. Chem. Phys., 11(9), 4547–4556, doi:10.5194/acp-11-4547-2011, 2011.

Damiani, A., Funke, B., López Puertas, M., Santee, M. L., Cordero, R. R. and Watanabe, S.: Energetic particle precipitation: A major driver of the ozone budget in the Antarctic upper stratosphere, Geophys. Res. Lett., 43(7), 3554–3562, doi:10.1002/2016GL068279, 2016.

Egorova, T., Rozanov, E., Zubov, V. and Karol, I.: Model for investigating ozone trends (MEZON), Izv. Atmos. Ocean. Phys., 39(3), 277–292, 2003.

Fischer, H., Birk, M., Blom, C., Carli, B., Carlotti, M., von Clarmann, T., Delbouille, L., Dudhia, A., Ehhalt, D., Endemann, M., Flaud, J. M., Gessner, R., Kleinert, A., Koopman, R., Langen, J., López-Puertas, M., Mosner, P., Nett, H., Oelhaf, H., Perron, G., Remedios, J., Ridolfi, M., Stiller, G. and Zander, R.: MIPAS: an instrument for atmospheric and climate research, Atmos. Chem. Phys., 8(8), 2151–2188, doi:10.5194/acp-8-2151-2008, 2008.

Froidevaux, L., Jiang, Y. B., Lambert, A., Livesey, N. J., Read, W. G., Waters, J. W., Browell, E. V., Hair, J. W., Avery, M. A., McGee, T. J., Twigg, L. W., Sumnicht, G. K., Jucks, K. W., Margitan, J. J., Sen, B., Stachnik, R. A., Toon, G. C., Bernath, P. F., Boone, C. D., Walker, K. A., Filipiak, M. J., Harwood, R. S., Fuller, R. A., Manney, G. L., Schwartz, M. J., Daffer, W. H., Drouin, B. J., Cofield, R. E., Cuddy, D. T., Jarnot, R. F., Knosp, B. W., Perun, V. S., Snyder, W. V., Stek, P. C., Thurstans,

5 R. P. and Wagner, P. A.: Validation of Aura Microwave Limb Sounder stratospheric ozone measurements, J. Geophys. Res. Atmos., 113(D15), D15S20, doi:10.1029/2007JD008771, 2008.

Funke, B., Lopez-Puertas, M., Stiller, G. P., Versick, S. and Von Clarmann, T.: A semi-empirical model for mesospheric and stratospheric NOy produced by energetic particle precipitation, Atmos. Chem. Phys., 16(13), 8667–8693, doi:10.5194/acp-16-8667-2016, 2016.

10 Fytterer, T., Mlynczak, M. G., Nieder, H., Pérot, K., Sinnhuber, M., Stiller, G. and Urban, J.: Energetic particle induced intra-seasonal variability of ozone inside the Antarctic polar vortex observed in satellite data, Atmos. Chem. Phys., 15(6), 3327–3338, doi:10.5194/acp-15-3327-2015, 2015.

Hitchcock, P., Shepherd, T. G. and Manney, G. L.: Statistical characterization of Arctic polar-night jet oscillation events, J. Clim., 26(6), 2096–2116, doi:10.1175/JCLI-D-12-00202.1, 2013.

15 Jackman, C. H., Marsh, D. R., Vitt, F. M., Garcia, R. R., Fleming, E. L., Labow, G. J., Randall, C. E., López-Puertas, M. and Funke, B.: Short- and medium-term atmospheric effects of very large solar proton events, Atmos. Chem. Phys. Discuss., 7(4), 10543–10588, doi:10.5194/acpd-7-10543-2007, 2007.

Jungclaus, J. H., Keenlyside, N., Botzet, M., Haak, H., Luo, J. J., Latif, M., Marotzke, J., Mikolajewicz, U. and Roeckner, E.: Ocean circulation and tropical variability in the coupled model ECHAM5/MPI-OM, J. Clim., 19(16), 3952–3972,

20 doi:10.1175/JCLI3827.1, 2006.

Livesey, N. J., Read, W. G., Wagner, P. A., Froidevaux, L., Lam- bert, A., Manney, G. L., Millán, L. F., Pumphrey, Hugh, C., Santee, M. L., Schwartz, M. J., Wang, S., Fuller, R. A., Jarnot, R. F., Knosp, B. W., and Martinez, E.: Version 4.2x Level 2 data quality and description document. Earth Observing System (EOS) Aura Microwave Limb Sounder (MLS), available at: https://mls.jpl.nasa.gov/data/v4-2_data_quality_document.pdf, last access: 6 April 2019

25 Maliniemi, V., Asikainen, T. and Mursula, K.: Spatial distribution of Northern Hemisphere winter temperatures during different phases of the solar cycle, J. Geophys. Res. Atmos., 119(16), 9752–9764, doi:10.1002/2013JD021343, 2014.

Marsh, D. R., Garcia, R. R., Kinnison, D. E., Boville, B. A., Sassi, F., Solomon, S. C. and Matthes, K.: Modeling the whole atmosphere response to solar cycle changes in radiative and geomagnetic forcing, J. Geophys. Res. Atmos., 112(23), 1–20, doi:10.1029/2006JD008306, 2007.

30 Marsland, S. J., Haak, H., Jungclaus, J. H., Latif, M. and Röske, F.: The Max-Planck-Institute global ocean/sea ice model with orthogonal curvilinear coordinates, Ocean Model., 5(2), 91–127, doi:10.1016/S1463-5003(02)00015-X, 2002.

Matthes, K., Funke, B., Andersson, M. E., Barnard, L., Beer, J., Charbonneau, P., Clilverd, M. A., Dudok De Wit, T., Haberreiter, M., Hendry, A., Jackman, C. H., Kretzschmar, M., Kruschke, T., Kunze, M., Langematz, U., Marsh, D. R., Maycock, A. C., Misios, S., Rodger, C. J., Scaife, A. A., Seppälä, A., Shangguan, M., Sinnhuber, M., Tourpali, K., Usoskin,

I., Van De Kamp, M., Verronen, P. T. and Versick, S.: Solar forcing for CMIP6 (v3.2), Geosci. Model Dev., 10(6), 2247–2302, doi:10.5194/gmd-10-2247-2017, 2017.

Mironova, I. A., Aplin, K. L., Arnold, F., Bazilevskaya, G. A., Harrison, R. G., Krivolutsky, A. A., Nicoll, K. A., Rozanov, E. V., Turunen, E. and Usoskin, I. G.: Energetic Particle Influence on the Earth's Atmosphere, Space Sci. Rev., 194(1–4), 1–96, doi:10.1007/s11214-015-0185-4, 2015.

Muthers, S., Anet, J. G., Stenke, A., Raible, C. C., Rozanov, E., Brönnimann, S., Peter, T., Arfeuille, F. X., Shapiro, a. I., Beer, J., Steinhilber, F., Brugnara, Y. and Schmutz, W.: The coupled atmosphere-chemistry-ocean model SOCOL-MPIOM, Geosci. Model Dev. Discuss., 7(3), 3013–3084, doi:10.5194/gmdd-7-3013-2014, 2014.

NOAA, ftp://ftp.swpc.noaa.gov/pub/indices/SPE.txt, last access on 6 April 2019

Pierrard, V. and Lopez Rosson, G.: The effects of the big storm events in the first half of 2015 on the radiation belts observed by EPT/PROBA-V, Ann. Geophys., 34(1), 75–84, doi:10.5194/angeo-34-75-2016, 2016.

Reddmann, T., Ruhnke, R., Versick, S. and Kouker, W.: Modeling disturbed stratospheric chemistry during solar-induced NOx enhancements observed with MIPAS/ENVISAT, J. Geophys. Res., 115, D00I11, doi:10.1029/2009JD012569, 2010.

Roeckner, E. and Bäuml, G.: The Atmospheric General Circulation Model ECHAM5 Model description, Max Plank Inst. Meteorol. Sci. Rep., (349), 1–127, 2003.

Rozanov, E., Calisto, M., Egorova, T., Peter, T. and Schmutz, W.: Influence of the Precipitating Energetic Particles on Atmospheric Chemistry and Climate, Surv. Geophys., 33(3–4), 483–501, doi:10.1007/s10712-012-9192-0, 2012.

Rozanov, E. V., Zubov, V. a., Schlesinger, M. E., Yang, F. and Andronova, N. G.: The UIUC three-dimensional stratospheric chemical transport model: Description and evaluation of the simulated source gases and ozone, J. Geophys. Res., 104, 11755, doi:10.1029/1999JD900138, 1999.

Schmidt, H., Brasseur, G. P., Charron, M., Manzini, E., Giorgetta, M. A., Diehl, T., Fomichev, V. I., Kinnison, D., Marsh, D. and Walters, S.: The HAMMONIA chemistry climate model: Sensitivity of the mesopause region to the 11-year solar cycle and CO2 doubling, J. Clim., 19(16), 3903–3931, doi:10.1175/JCLI3829.1, 2006.

Semeniuk, K., Fomichev, V. I., McConnell, J. C., Fu, C., Melo, S. M. L. L. and Usoskin, I. G.: Middle atmosphere response to the solar cycle in irradiance and ionizing particle precipitation, Atmos. Chem. Phys., 11(10), 5045–5077, doi:10.5194/acp-11-5045-2011, 2011.

Seppälä, A., Lu, H., Clilverd, M. A. and Rodger, C. J.: Geomagnetic activity signatures in wintertime stratosphere wind, temperature, and wave response, J. Geophys. Res. Atmos., 118(5), 2169–2183, doi:10.1002/jgrd.50236, 2013.

Sheese, P. E., Walker, K. A., Boone, C. D., McLinden, C. A., Bernath, P. E., Bourassa, A. E., Burrows, J. P., Degenstein, D. A., Funke, B., Fussen, D., Manney, G. L., Thomas McElroy, C., Murtagh, D., Randall, C. E., Raspollini, P., Rozanov, A., Russell, J. M., Suzuki, M., Shiotani, M., Urban, J., Von Clarmann, T. and Zawodny, J. M.: Validation of ACE-FTS version 3.5 NOy species profiles using correlative satellite measurements, Atmos. Meas. Tech., 9(12), 5781–5810, doi:10.5194/amt-9-5781-2016, 2016.

Sinnhuber, M., Berger, U., Funke, B., Nieder, H., Reddmann, T., Stiller, G., Versick, S., Von Clarmann, T. and Wissing, J.

M.: NOyproduction, ozone loss and changes in net radiative heating due to energetic particle precipitation in 2002-2010, Atmos. Chem. Phys., 18(2), 1115–1147, doi:10.5194/acp-18-1115-2018, 2018.

Solomon, S., Crutzen, P. J. and Roble, R. G.: Photochemical coupling between the thermosphere and the lower atmosphere: 1. Odd nitrogen from 50 to 120 km, J. Geophys. Res., 87, 7206, doi:10.1029/JC087iC09p07206, 1982.

5 SPARC: The SPARC Data Initiative: Assessment of stratospheric trace gas and aerosol climatologies from satellite limb sounders. M. I. Hegglin and S. Tegtmeier (Eds.), SPARC Report No. 8, WCRP-05/2017, doi:10.3929/ethz-a-010863911, 2017.

Stenke, A., Schraner, M., Rozanov, E., Egorova, T., Luo, B. and Peter, T.: The SOCOL version 3.0 chemistry-climate model: Description, evaluation, and implications from an advanced transport algorithm, Geosci. Model Dev., 6(5), 1407–1427, doi:10.5194/gmd-6-1407-2013, 2013.

10 Turunen, E., Verronen, P. T., Seppälä, A., Rodger, C. J., Clilverd, M. A., Tamminen, J., Enell, C. F. and Ulich, T.: Impact of different energies of precipitating particles on NOx generation in the middle and upper atmosphere during geomagnetic storms, J. Atmos. Solar-Terrestrial Phys., 71(10–11), 1176–1189, doi:10.1016/j.jastp.2008.07.005, 2009.

Verronen, P. T. and Lehmann, R.: Enhancement of odd nitrogen modifies mesospheric ozone chemistry during polar winter, Geophys. Res. Lett., 42(23), 10445–10452, doi:10.1002/2015GL066703, 2015.

15 Waters, J. W., Froidevaux, L., Harwood, R. S., Jarnot, R. F., Pickett, H. M., Read, W. G., Siegel, P. H., Cofield, R. E., Filipiak, M. J., Flower, D. A., Holden, J. R., Lau, G. K., Livesey, N. J., Manney, G. L., Pumphrey, H. C., Santee, M. L., Wu, D. L., Cuddy, D. T., Lay, R. R., Loo, M. S., Perun, V. S., Schwartz, M. J., Stek, P. C., Thurstans, R. P., Boyles, M. A., Chandra, K. M., Chavez, M. C., Chen, G. S., Chudasama, B. V., Dodge, R., Fuller, R. A., Girard, M. A., Jiang, J. H., Jiang, Y., Knosp, B. W., Labelle, R. C., Lam, J. C., Lee, K. A., Miller, D., Oswald, J. E., Patel, N. C., Pukala, D. M., Quintero, O., Scaff, D. M.,

20 Van Snyder, W., Tope, M. C., Wagner, P. A. and Walch, M. J.: The Earth Observing System Microwave Limb Sounder (EOS MLS) on the aura satellite, IEEE Trans. Geosci. Remote Sens., 44(5), 1075–1092, doi:10.1109/TGRS.2006.873771, 2006.

Wissing, J. M. and Kallenrode, M. B.: Atmospheric ionization module Osnabrück (AIMOS): A 3-D model to determine atmospheric ionization by energetic charged particles from different populations, J. Geophys. Res. Sp. Phys., 114(6), 1–14, doi:10.1029/2008JA013884, 2009.

25 Yando, K., Millan, R. M., Green, J. C. and Evans, D. S.: A Monte Carlo simulation of the NOAA POES Medium Energy Proton and Electron Detector instrument, J. Geophys. Res. Sp. Phys., 116(10), 1–13, doi:10.1029/2011JA016671, 2011.
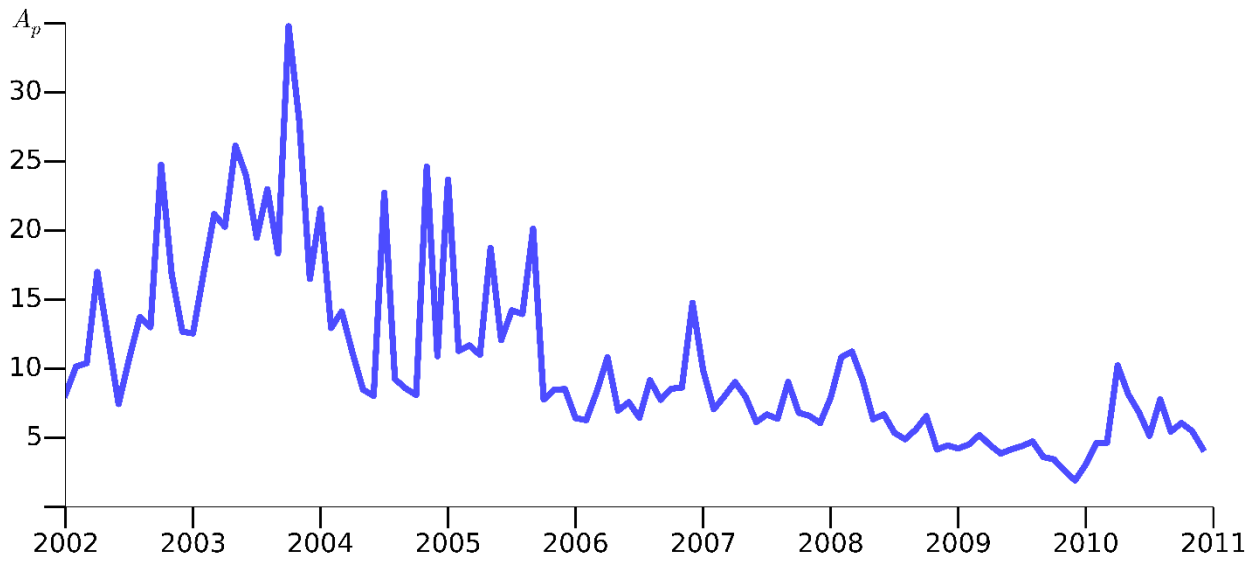
Figure 1: The monthly mean geomagnetic A$_p$ index during the simulated period: Years 2002 – 2005 were rather active, while the period 2006 – 2010 was geomagnetically quiescent (CMIP-6 dataset; Matthes *et al* 2017).
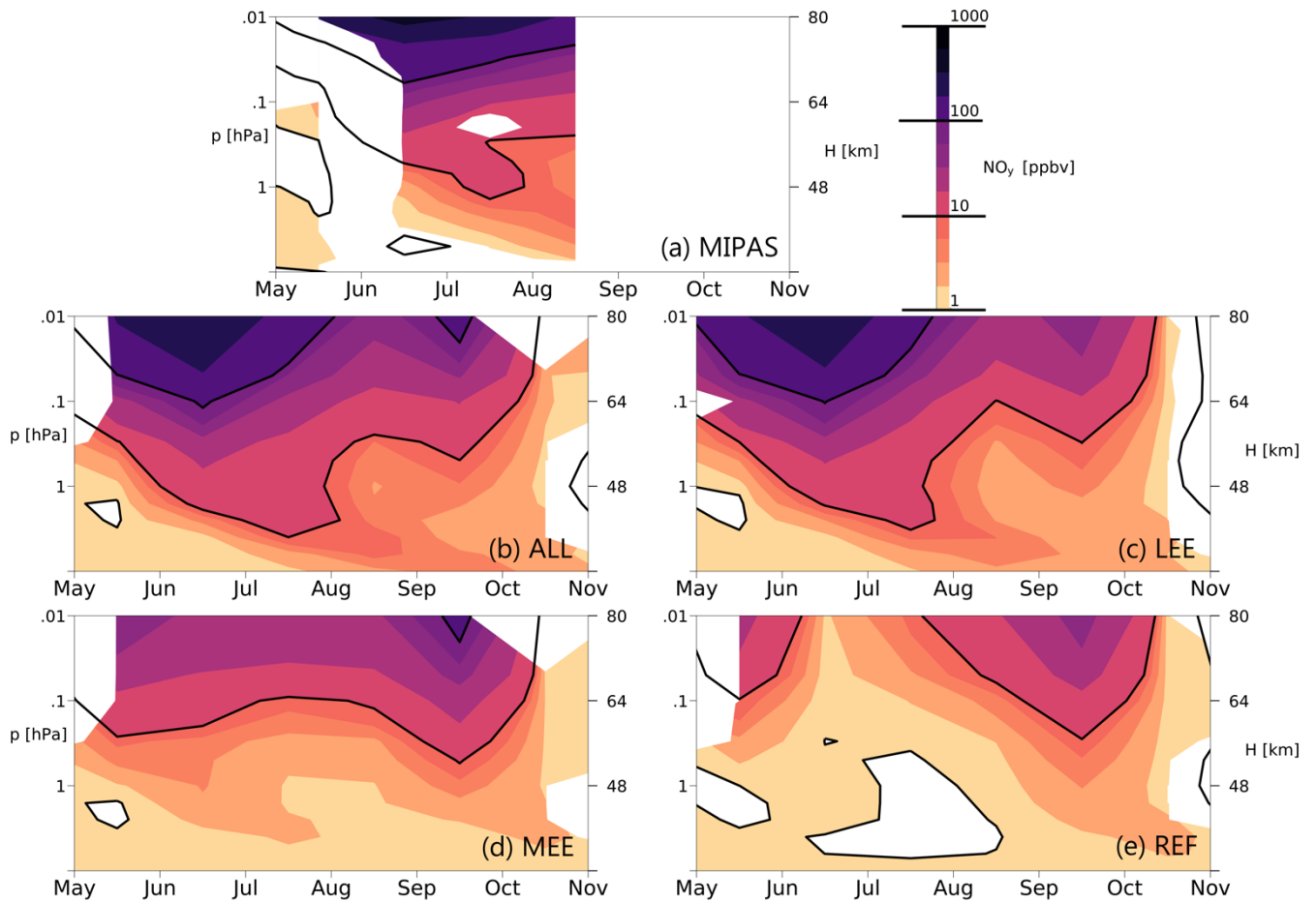
Figure 2: Monthly mean NO$_y$ volume mixing ratio anomaly in ppbv for the Southern Hemisphere (> 70° S average) calculated as difference of the year 2005 and the average of 2006 – 2010. (a) MIPAS observations; (b) ensemble mean of ALL simulations; (c) ensemble mean of LEE simulations; (d) ensemble mean of MEE simulations; (e) ensemble mean of REF simulations. Color levels are 1, 2.5, 5, 7.5, 10, 25, 50, 75, 100, 250, 500, 750 and 1000 ppbv and the black contour lines highlight 1, 10, 100 and 1,000 ppbv. Colored regions are significant at the 99 % confidence level (calculated using a Student t-test).
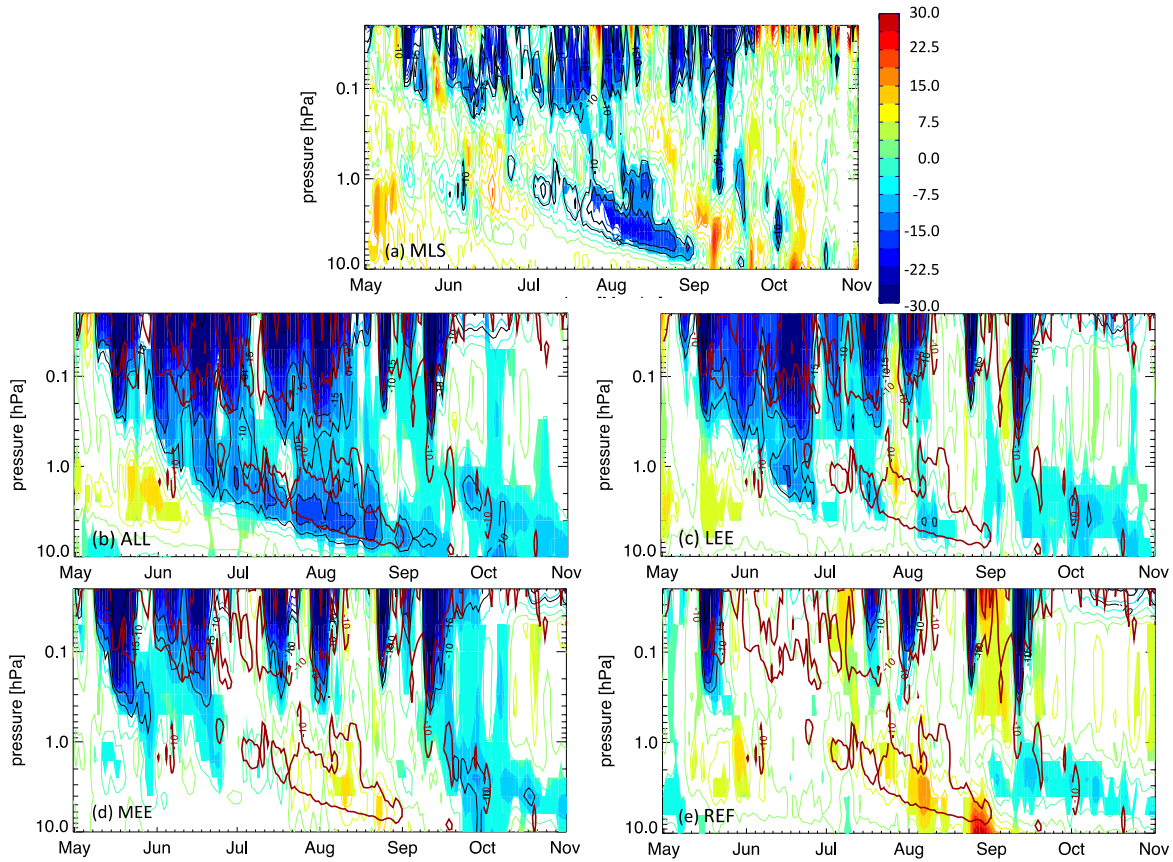
Figure 3: Monthly mean ozone anomaly poleward of 70° S calculated as difference of year 2005 and average of 2006 – 2010 relative to 2005 – 2010 period. (a) MLS observations; (b) ensemble mean of ALL simulations; (c) ensemble mean of LEE simulations; (d) ensemble mean of MEE simulations; (e) ensemble mean of REF simulations. Black lines highlight -10 %, -15% and -50 % and dark red lines mark -10 % from MLS observations on every plot. Note that mesospheric ozone depletion reaches 80-90 % during some strong solar proton events. Colored regions are significant at the 99 % confidence level (calculated using a Student t-test).
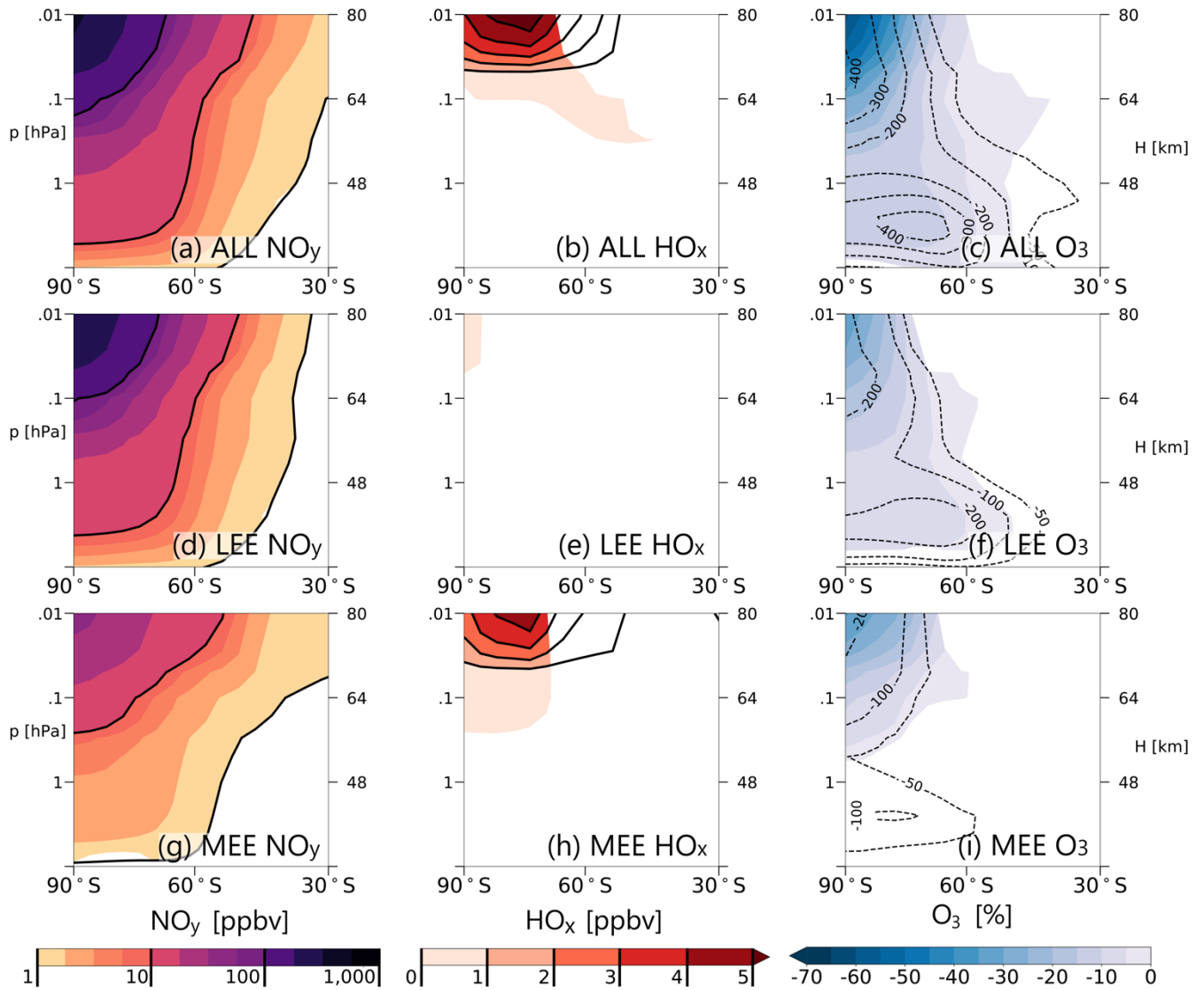
Figure 4: Summary of zonally averaged results. Columns: NO_y (left); HO_x (center); O_3 (right). Rows: including ALL energetic particles (top); only with LEE (center); only with MEE (bottom). All panels show results for the geomagnetically active period (2002 – 2005) for austral winter (JJA) from the respective simulations minus the REF simulation. Colors show absolute differences in ppbv for NO_y (color levels are 1, 2.5, 5, 7.5, 10, 25, 50, 75, 100, 250, 500, 750 and 1000 ppbv) and HO_x plots and difference in percent for O_3 plots. Isolines show difference in absolute values in ppbv. Colored regions are significant at the 99 % confidence level (calculated using a Student t-test).